THE ASTROPHYSICAL JOURNAL, 524:1105–1121, 1999 October 20

OBSERVATION AND MODELING OF THE SOLAR TRANSITION REGION. I. MULTI-SPECTRAL SOLAR TELESCOPE ARRAY OBSERVATIONS

HAKEEM M. OLUSEYI
Department of Physics and Center for Space Sciences and Astrophysics, Stanford University, Stanford, CA 94305-4060; Hakeem@banneker.stanford.edu
A. B. C. WALKER II
Departments of Physics and of Applied Physics, Stanford University, Stanford, CA 94305-4060; walker@banneker.stanford.edu
JASON PORTER AND RICHARD B. HOOVER
Space Sciences Laboratory, NASA Marshall Space Flight Center, Huntsville, AL 35812; Jason.Porter@msfc.nasa.gov, Richard.Hoover@msfc.nasa.gov
AND
TROY W. BARBEE, JR.
Chemistry and Materials Science Department, Lawrence Livermore National Laboratory, Livermore, CA; barbee2@llnl.gov
Received 1998 December 3; accepted 1999 May 13

ABSTRACT

We report on observations of the solar atmosphere in several extreme-ultraviolet and far-ultraviolet bandpasses obtained by the Multi-Spectral Solar Telescope Array, a rocket-borne spectroheliograph, on flights in 1987, 1991, and 1994, spanning the last solar maximum. Quiet-Sun emission observed in the 171–175 Å bandpass, which includes lines of O V, O VI, Fe IX, and Fe X, has been analyzed to test models of the temperatures and geometries of the structures responsible for this emission. Analyses of intensity variations above the solar limb reveal scale heights consistent with a quiet-Sun plasma temperature of $500{,}000 \leq T_e \leq 800{,}000$ K. The structures responsible for the quiet-Sun EUV emission are modeled as small quasi-static loops. We submit our models to several tests. We compare the emission our models would produce in the bandpass of our telescope to the emission we have observed. We find that the emission predicted by loop models with maximum temperatures between 700,000 and 900,000 K are consistent with our observations. We also compare the absolute flux predicted by our models in a typical upper transition region line to the flux measured by previous observers. Finally, we present a preliminary comparison of the predictions of our models with diagnostic spectral line ratios from previous observers. Intensity modulations in the quiet Sun are observed to occur on a scale comparable to the supergranular scale. We discuss the implications that a distribution of loops of the type we model here would have for heating the local network at the loops' footpoints.

Subject headings: Sun: chromosphere — Sun: transition region — Sun: UV radiation

1. INTRODUCTION

Solar plasmas in the temperature range ~20,000–1,000,000 K, intermediate between the temperature of the chromosphere and that of the corona, are referred to as the "transition region." As the name implies, early models of the solar atmosphere (Giovanelli 1949) assumed that these plasmas, which radiate most strongly in the far-ultraviolet (FUV) and extreme-ultraviolet (EUV) lines of ions such as H I, He I–II, C II–IV, N II–V, O II–VI, Ne II–VIII, Mg III–IX, Si III–IX, S III–IX, and Fe VI–IX, are physically interposed between coronal structures and the chromosphere. However, models of large-scale coronal loops (Vesecky, Antiochos, & Underwood 1979), the structures that contain the coronal plasma with $T > 1{,}000{,}000$ K, have shown that the emission measure of the plasma at their footpoints, where a transition to chromospheric temperatures occurs, is insufficient to explain the magnitude of the EUV and FUV emission of the solar atmosphere (Athay 1981a, 1981b, 1984; Rabin & Moore 1984; Dowdy, Emslie, & Moore 1987).

A number of structures have been proposed as the site of the "transition region" plasma. In the model of Gabriel (1976), transition-region plasma is magnetically supported by the field associated with the supergranular network (hereafter called the network) and is connected to the network by magnetic funnels having unipolar configurations. In Gabriel's model, the transition-region plasma should show a strong correlation with the magnetic structure of the network, but it is also connected to plasmas at coronal temperatures. Rabin (1991) has analyzed the energy balance in coronal funnels such as those postulated by Gabriel. Rabin concludes that the structure of funnels with peak temperature greater than 1,000,000 K can account for the emission measure necessary to generate the hotter transition-region emission in lines such as O VI and Ne VII, but, like loops with peak temperatures above 1,000,000 K, cannot account for the magnitude or temperature distribution of the emission generated below 100,000 K. Rabin's analysis does not exclude the possibility that funnels with a lower peak temperature may contribute to the transition-region plasma.

In a series of papers, Feldman (1983, 1987) suggested that the features observed by the High Resolution Telescope Spectrograph (HRTS) instrument in lines emitted between 40,000 and 500,000 K represent the structures responsible for transition-region emission. He concludes that these structures must be thermally and magnetically isolated from both the chromosphere and the corona. He referred to the structures responsible for this emission as "unresolved fine structure." Focusing more narrowly on the lines emitted by the lower transition region, Dowdy, Rabin, & Moore (1986) and Antiochos & Noci (1986) have proposed that low-lying small (<10,000 km) "cool" loops with maximum temperature $T_m < 100{,}000$ K, located in the mag-

netic lanes of the network, might contain the lower transition region plasma. If they were found to exist, these cool loops would presumably not be thermally connected to the material in the much hotter coronal loops. In support of this hypothesis, Antiochos & Noci developed models suggesting that in addition to the solutions that describe the well known hot coronal loops with $T_m > 1{,}000{,}000$ K, low-lying loops with $T_m < 100{,}000$ K would also be stable. Both groups of authors suggested that cool loops might be the source of the lower transition region EUV emission in lines such as C IV and He II, and of the emission in the strongest line, H Lyα, which, according to Fontenla, Avrett, & Loeser (1990, 1991, 1993), is emitted from plasmas in the temperature range of 20,000–70,000 K. However, Cally & Robb (1991) have argued that cool loops are not stable, and are either rapidly heated to $T > 250{,}000$ K or cooled to $T \sim 20{,}000$ K, depending on the relationship between their mass and the energy dissipated in the loop. The analysis of Cally & Robb does permit the existence of loops with $250{,}000 < T_m < 1{,}000{,}000$ K. In the present paper, we will explore the possible contribution of such loops, which we refer to as "lukewarm loops," to upper transition region ($10^5 < T_e < 10^6$ K) emission, and the contribution these loops would make to lower transition region ($20{,}000 < T_e \leq 100{,}000$ K) emission via thermal conduction. We note that recently, Fludra et al. (1997) have argued that the majority of the EUV emission excited in the temperature range from $\sim$80,000 to 800,000 K comes from loops and other unresolved structures that do not reach coronal temperatures ($T > 1{,}000{,}000$ K).

One of the characteristics of the magnetic structure of the network cited by Dowdy et al. (1986) and Dowdy (1993) in support of their suggestion that cool loops are present in the network is that the discrete magnetic elements that make up the network include both polarities in close proximity. At the time that Dowdy et al. (1986) and Dowdy (1993) made their proposals, loops with their footpoints embedded in the network had not been observed. Recently, Kankelborg et al. (1996, 1997) have analyzed FUV observations of lower transition region structures in the emission of H Lyα (1216 Å) and EUV and soft X-ray observations of coronal structure in narrow wavelength bands dominated by the emission of Fe IX/X (171–175 Å), Fe XII (186–200 Å), Fe XIV (206–216 Å), and Si XII (43.5–45 Å), obtained by the Multi-Spectral Solar Telescope Array (MSSTA), a rocket-borne spectroheliograph (Walker et al. 1990a). Kankelborg et al. (1996, 1997) observed 26 small loops in the soft X-ray images; the footpoints of all 26 loops coincide with network elements that are brighter than average in the H Lyα images. The footpoints of 18 of these loops are coincident with magnetic bipoles in the Kitt Peak magnetogram taken 4 hr before the launch of the MSSTA. The magnetic configuration of the footpoints of the other eight loops is difficult to determine because they are close to the limb. A typical loop and its footpoints are shown in Figure 1. An analysis of these loops, which vary in size from 7000 to 70,000 km, shows that the maximum loop temperature, T_m, is typically 1,200,000 to 2,000,000 K, permitting Kankelborg et al. (1996, 1997) to identify them as "coronal X-ray bright points" (XBPs; Golub 1980). Kankelborg et al. have developed loop models for the 26 XBP's they observed, which show that for a typical XBP the thermal flux conducted below the 100,000 K isotherm (approximately 50% of the energy dissipated in the loop) is sufficient to supply the energy radiated in the H Lyα line by the local network. Less than 1% of the bright elements that form the network in H Lyα emission are at the footpoints of XBP's; these elements, however, are the brightest elements, and are located over the most intense magnetic fields in the network. In a series of papers, Fontenla, Avrett, & Loeser (1990, 1991, 1993; hereafter FAL) have considered the structure of the lower transition region (LTR). Their models show that conductive heat fluxes compatible with those found by Kankelborg et al. can be dissipated by radiative losses in the lower transition region, with H Lyα as the principle energy-loss mode. In their analyses, FAL assume that the top of the LTR (taken to be 10^5 K) is the interface of the chromosphere with coronal plasmas with $T > 10^6$ K. It is possible, however, that the LTR modeled by FAL is the interface of chromospheric material with plasma at subcoronal temperatures, since the only constraint on the plasma lying above 10^5 K is that the heat flux from these plasmas match that of the FAL models.

Recently, Falconer et al. (1996, 1998) have reported on observations by the *SOHO* EUV Imaging Telescope (EIT) experiment of "microcoronal bright points," less than 10″ ($\sim$7000 km) in size, that are rooted in small-scale magnetic bipoles in the network. Pres & Phillips (1999) also used observations by the *SOHO* EIT experiment to explore the relationship of XBPs to the dynamics of small-scale magnetic bipoles in the quiet Sun, and suggest that the dissipation of magnetic energy can account for the energy

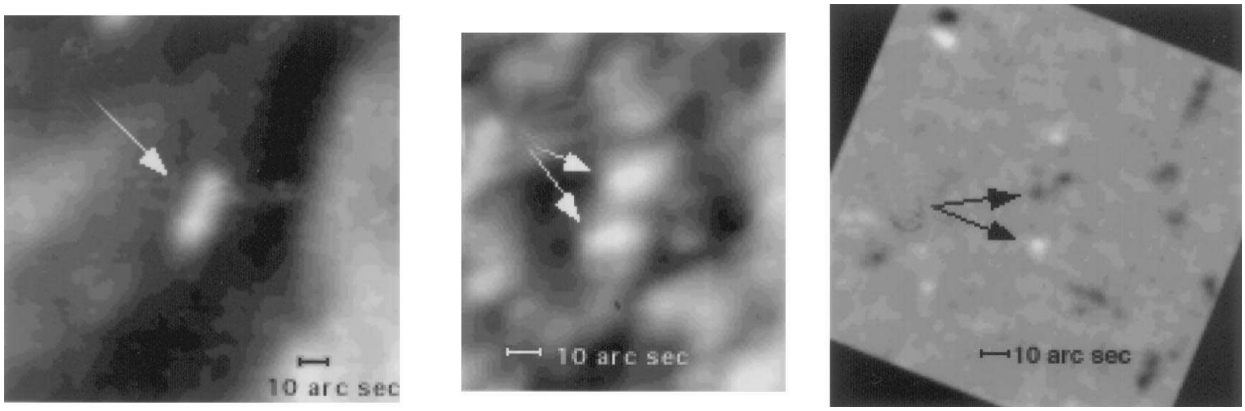

FIG. 1.—*Left*: Coronal X-ray bright point observed in the emission of Fe XII ($\sim$193 Å) by the MSSTA in 1991. *Middle*: Lower transition footpoints of the bright point observed in H Lyα. *Right*: Line-of-sight magnetic field observed by the Kitt Peak magnetograph 4.5 hr before the MSSTA launch. The magnetogram has been rotated to compensate for the time difference in the observations. (From Kankelborg et al. 1996.)

radiated and conducted to cooler plasmas by these loops. The analysis of Prés & Phillips, in particular, emphasizes the importance of conductive flux. These observations extend the relationship between the network and coronal bright points to smaller and fainter structures than those studied by Kankelborg et al.

The analyses of Kankelborg et al. (1996, 1997), Falconer et al. (1996, 1998), and Pres & Phillips (1999) are based on observations obtained in a bandpass centered on the lines of Fe XII at 193 Å. We find that there is also a strong correlation between the network and diffuse emission observed in the images recorded in the bandpass from 171 to 175 Å. This bandpass is dominated by emission lines of Fe IX and Fe X, which are excited between 500,000 and 1,300,000 K. There are also lines of O V and O VI, which are excited between 200,000 and 400,000 K, in this bandpass. In the current paper we present evidence that the plasma responsible for the diffuse emission observed in the MSSTA 171–175 Å images is at a temperature of ~250,000–900,000 K and is associated with the network. We note that analysis of observations obtained by the Harvard Spectrophotometer on *Skylab* (Reeves et al. 1976, 1977) have shown that network structure can be observed in the emission of Ne VII 465 Å, which is excited at temperatures as high as 700,000 K (Reeves 1976; Dowdy 1993). In fact, Dowdy states that "some fraction of the quiet-Sun EUV output is generated within network loops that are effectively insulated from the corona."

Our observations differ from the Harvard *Skylab* observations (Reeves et al. 1977) in several respects: they have higher angular resolution (~2″–5″, compared to ~5″–10″) and they cover the entire solar disk.[1] However, the MSSTA observations do not have full coverage of the transition region in temperature, and their interpretation is complicated by lower spectral resolution, which does not permit a single emission line to be isolated. More recent observations with the SUMER experiment on board *SOHO* reveal network structure in full-disk images obtained in the emission of 13 lines formed between 10,000 and 200,000 K, with a spatial resolution of 2″ and a 44 mÅ spectral resolution (Wilhelm et al. 1998). The SUMER experiment has also obtained a full-disk image in the emission of Ne VIII (770.41 Å) formed at ~630,000 K (Wilhelm et al. 1998). While the network structure is visible in this image, the image is dominated by an unresolved diffuse emission covering much of the solar disk, which is absent from the images formed at temperatures at or below 200,000 K. Furthermore, an image obtained by the EIT experiment on board *SOHO*, in a bandpass centered at 284 Å (Fe XV) corresponding to plasma at ~2,000,000 K, taken on the same day as the SUMER Ne VIII image, is dominated primarily by bright active regions.[2] Each of these observations appears to support the existence of a component of the solar atmosphere that is related to the network, somewhat cooler than the corona, and not directly connected to the corona.

2. OBSERVATIONS

One of the advantages of normal incidence multilayer optics for the study of the solar atmosphere (Plummer et al. 1995; Walker et al. 1990b; Barbee 1990) is that multilayers permit the selection of a relatively narrow wavelength range (typically $\lambda/\Delta\lambda \sim 20$–100), permitting a more precise analysis of thermal structure than is possible with, for example, grazing-incidence Wolter optics. We have obtained multilayer images of chromospheric, transition-region, and coronal structures in three rocket flights covering the period 1987–1994, which roughly encompasses a maximum in the solar cycle and the preceding and following minima. Our coronal observations include the following bandpasses: 171–175 Å, which is dominated by the resonance lines of Fe IX and Fe X, excited at ~500,000–1,300,000 K; 171–185 Å, which is sensitive to Fe IX, Fe X, and Fe XI emission, excited at ~500,000–1,600,000 K; 190–205 Å, which is dominated by lines of Fe XII and Fe XIII, excited at 1,000,000–2,000,000 K; and 279–289 Å, which is dominated by lines of Fe XV, excited at ~1,200,000–2,750,000 K. Our 1987 observations (Walker et al. 1988) in the 171–175 Å bandpass contained an unexpected feature. In addition to active-region loops, polar plumes, and XBPs, which are well-known features of the coronal plasma above 1,000,000 K, we observed emission covering virtually the entire solar disk (Fig. 2). This emission, which has an intensity modulation on a spatial scale of 20,000–30,000 km, appears to be related to the network (this relationship is discussed further in § 4.4). Because of the presence of weak lines of O V and O VI, which are excited at temperatures in the range 200,000–400,000 K, in the 171–175 Å bandpass (Fig. 3), the interpretation of these observations based on the 1987 images alone is ambiguous. Did we observe material at coronal or subcoronal temperatures ($500{,}000 \leq T_e < 1{,}000{,}000$ K) that was magnetically connected to the supergranular network, did we observe transition region structures at ~300,000 K, or did we observe material spanning both temperature regimes?

In 1991 we again observed the corona and chromosphere, this time near solar maximum (Walker et al. 1993b). Our 1991 171–175 Å and 190–205 Å bandpass images (Figs. 4 and 5) were strongly dominated by active regions and by XBPs. The diffuse general disk emission that was so prominent in 1987, although still visible, was less dominant (Fig. 4*a*); the network structure visible in Figure 2 is also less prominent, but is visible in Figure 4*b*, which has higher angular resolution than Figure 4*a*. Analysis of XBPs and polar plumes observed in the 190–205 Å image and of the underlying lower transition structure as observed in H Lyα (Fig. 6) resulted in the following models of the chromosphere/corona interface:

1. The magnetic structure of the footpoints of polar plumes is predominately monopolar on scales of 7000–20,000 km (~10″–30″ as observed from the earth), their thermal structure is consistent with the thesis that the lower transition region emission at their footpoints is generated by conduction from the corona, and the H Lyα signatures of the network elements at the footpoints of plumes are distinguished from other network elements in the coronal hole by being brighter (Allen et al. 1997).[3] Furthermore, models of the thermal and density structure of polar plumes based on our observations have been shown to be consistent with the thesis that while polar plumes are not the source of high-speed solar wind streams, as structures of enhanced density in the predominantly open magnetic configuration of

[1] The optical performance tests of the MSSTA telescopes are described by Hoover et al. (1990a, 1990b) and Martinez-Galarce et al. (1998).

[2] This image can be viewed at: http://soho01.nascom.nasa.gov/summary/gif/960202/seit_00284_fd_19960202_1444.gif.

[3] We note, however, that bipolar structure has been reported in coronal holes on the scale of 1″–2″ (see Wang & Sheeley 1995; Wang et al. 1997a).

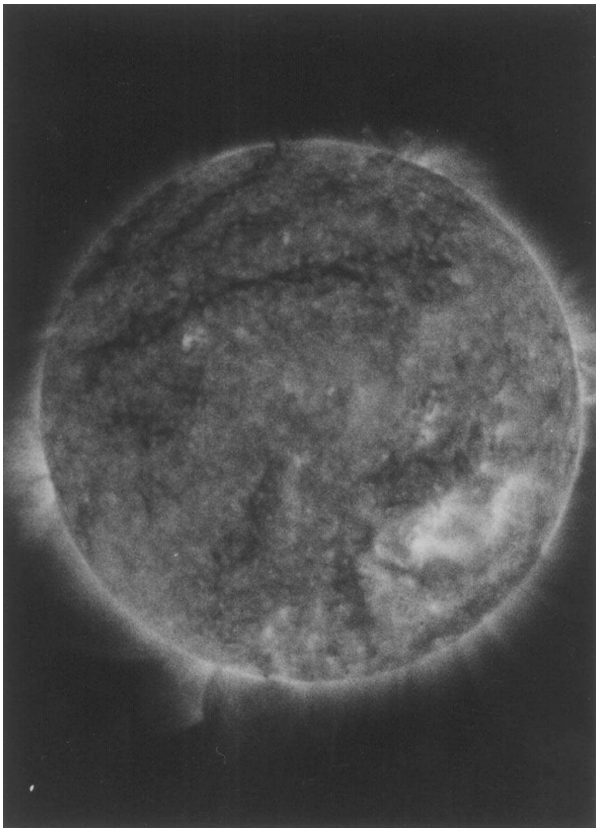

FIG. 2*a*

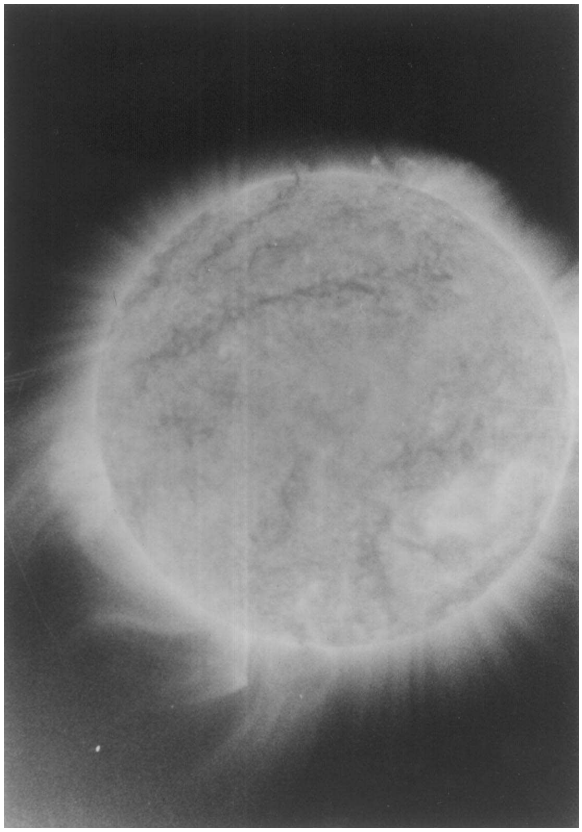

FIG. 2*b*

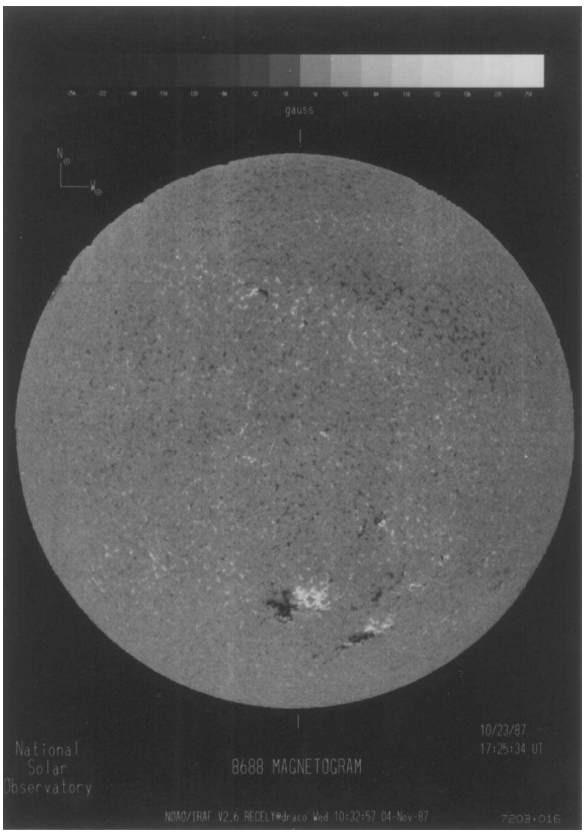

FIG. 2*c*

FIG. 2.—(*a*) Corona as observed in the 171–175 Å bandpass (Fe IX/X) with a Cassegrain multilayer telescope by Walker et al. (1988). This figure shows the diffusion emission on the disk that appears to have structures on the same scale as the supergranulation. (*b*) This image is presented to emphasize the large-scale plumes and other structures above the limb that are visible in this bandpass. (*c*) Magnetogram taken at KPNO simultaneously with our rocket flight.

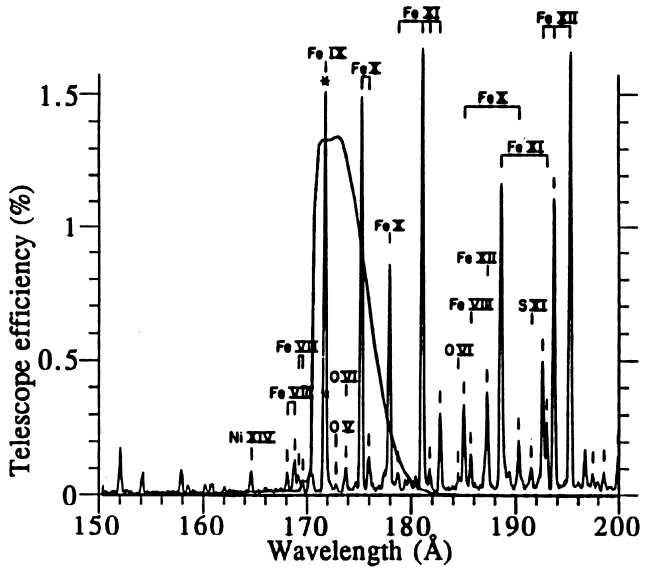

FIG. 3.—Wavelength response of the 171–175 Å telescope flown in 1987, superimposed on the coronal spectrum as measured by Malinovsky & Heroux (1973).

coronal holes, they contribute significantly to solar wind particle fluxes (Allen et al. 1997).

2. XBPs are small loops, typically 7000–20,000 km long (10″–30″), and their footpoints are located at the poles of bipolar magnetic structures that are embedded in the network. The H Lyα signatures of the network elements at the footpoints of XBPs are distinguished from other network elements in the quiet Sun and in coronal holes by being brighter (Kankelborg et al. 1996, 1997). Loop models derived for 26 XBPs are consistent with the thesis that the lower transition region emission at their footpoints is generated by thermal heat conduction from the corona (Kankelborg et al. 1996, 1997).

The network as observed in H Lyα emission consists of thousands of discrete elements that are ~5″ or less in diameter (we note that it is possible that these elements are formed by the fusion of smaller magnetic structures that originate in the photosphere; Berger et al. 1995, 1998; Berger & Title 1996). The network as observed by the MSSTA in H Lyα in 1991 is shown in Figure 6. Based on the analyses cited above, we conclude that the brightest network elements are associated with the footpoints of XBPs (Kankelborg et al. 1996, 1997) and coronal loops (Oluseyi 1999) in the quiet Sun, and with the footpoints of plumes (Allen et al. 1997; Wang & Sheeley 1995) and XBPs (Kankelborg et al. 1996, 1997) in coronal holes. However, the majority of the network elements observed in H Lyα emission are not clearly identified with a discrete coronal structure.

In 1994, which was again near solar minimum, we obtained images in the 171–175 Å bandpass (Fig. 7), in the 171–185 Å bandpass, in the 279–289 Å bandpass (Fig. 8), in a bandpass centered at 1550 Å, which includes the resonance line of C IV (Fig. 9), and in a bandpass centered at 1216 Å (Fig. 10). The 171–175 Å image again shows diffuse emission covering most of the solar disk; in sharp contrast, the 279–289 Å image shows emission that is mostly confined to active-region loops. The 1216 Å H Lyα image and the 1550 Å image, which includes the 1600 Å continuum from the temperature minimum on the disk, the resonance lines of C IV, and lines of low-excitation ions such as Fe II and Si II, each show very strong network structure that is closely related to the magnetic network (Fig. 11).

3. ANALYSIS

In this section we discuss the analysis of the 1987 and 1994 MSSTA rocket observations and develop a model of

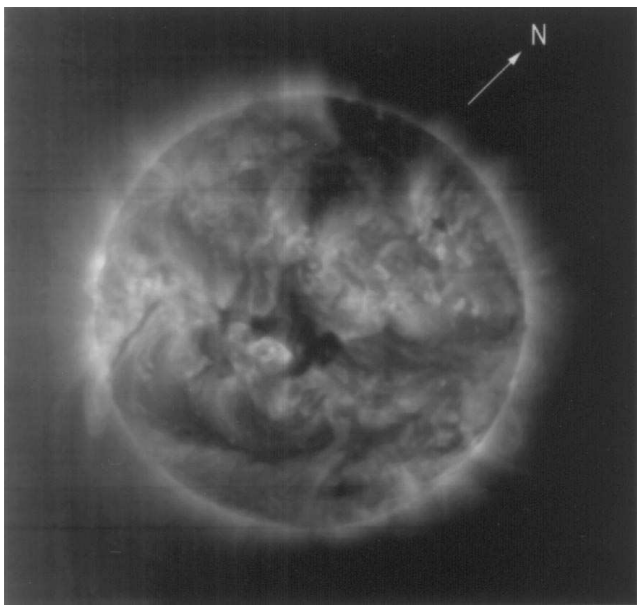

FIG. 4*a*

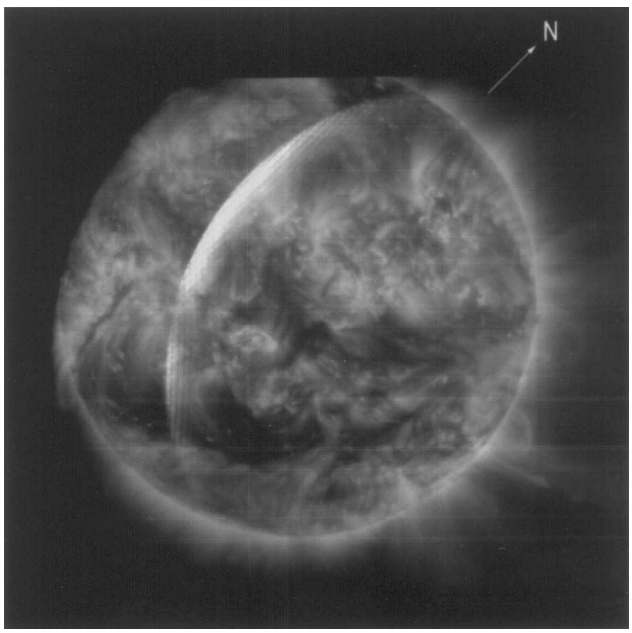

FIG. 4*a*

FIG. 4.—(*a*) Corona in the 171–175 Å bandpass (Fe IX/X) as observed in 1991 (Walker et al. 1993a) with a Cassegrain telescope. (*b*) Corona in the 171–175 Å bandpass observed with a Ritchey-Chretién multilayer telescope. This telescope was damaged on launch, causing the misalignment of the optical baffle. The superior resolution of the Ritchey-Chretién optical design and the use of higher resolution film permit the spatial modulation of the diffuse emission to be more readily observed in this image than in (*a*).

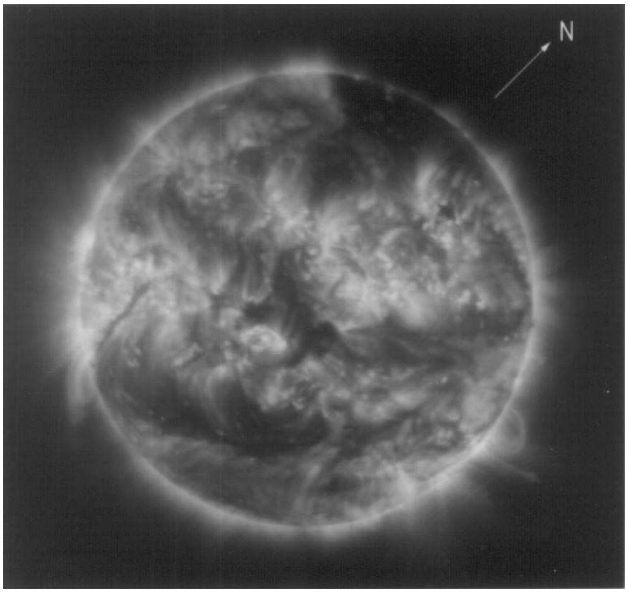

FIG. 5.—Corona in the 190–205 Å bandpass (Fe XII) as observed in 1991 (Walker et al. 1993a)

the diffuse emission observed in our 171–175 Å image from 1987.

3.1. *Instrument Response*

The energy density, D, at point (x, y) in the image of an optically thin plasma produced by a multilayer telescope is given by DeForest et al. (1991) as

$$D_n(x, y) = \frac{1}{4\pi f^2}\,\frac{\pi}{4}\,(A^2 - a^2)a_{\rm H}\int_{T_0}^{T} dT_e\,K_n(T_e)n_e^2(T_{e,x,y})\,, \tag{1}$$

where A and a are the apertures of the primary and secondary mirrors, $V(x, y)$ is the vignetting function of the telescope, f is the focal length of the telescope, and x and y represent solar coordinates (which are mapped onto the image plane). The solar plasma is described by $a_{\rm H}$, the number of electrons per hydrogen atom (assumed to be constant), and $n_e^2(T_e)$, the emission measure at electron temperature T_e that is characteristic of the solar structure under study. The "kernel" of the integral equation, $K_n(T_e)$, which is the convolution of the telescope efficiency $\epsilon(\lambda_{ij})$ and the solar emissivity, is given by

$$K_n(T_e) = \sum_{Zzij}(hc)A_z\,\epsilon(\lambda_{ij})a_{Zzij}(T_e)\alpha_{Zzij}(T_e)\alpha_{Zzij}(T_e)\,, \tag{2}$$

where A_Z is the abundance of element Z, a_{Zz} is the fractional population of ionization stage z, and α_{Zzij} is the excitation function for transition $(i–j)$ (including all population pro-

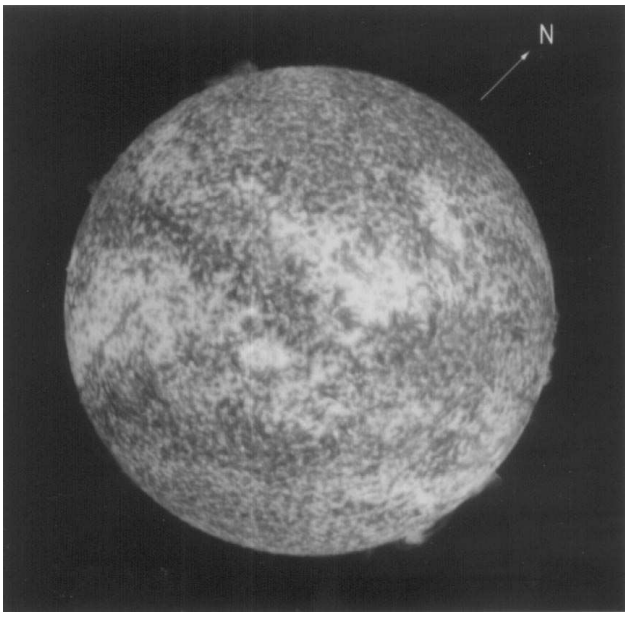

FIG. 6*a*

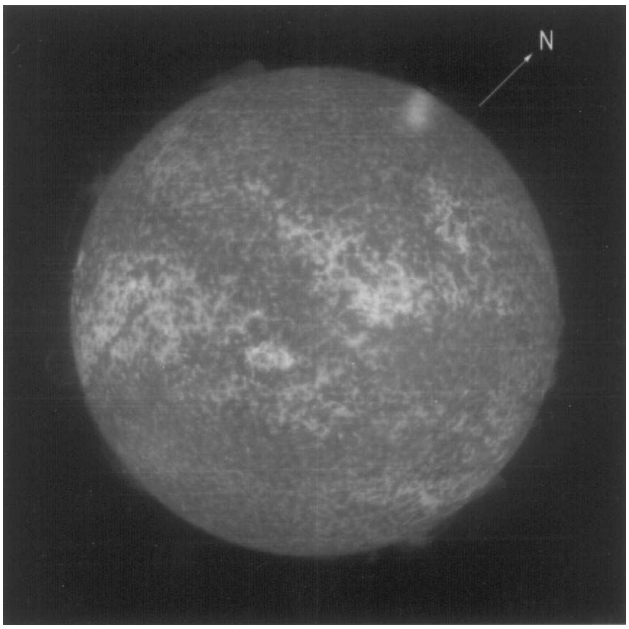

FIG. 6*b*

FIG. 6.—(*a*) Lower transition region in H Lyα emission as observed in 1991, recorded on Kodak 649 emulsion. Note that the network is resolved into discrete bright structures typically $\sim$25 arcsec^2 in area. (*b*) Lower transition in H Lyα emission as observed in 1991, recorded on Kodak XUV 100 emulsion. This image has lower resolution than (*a*).

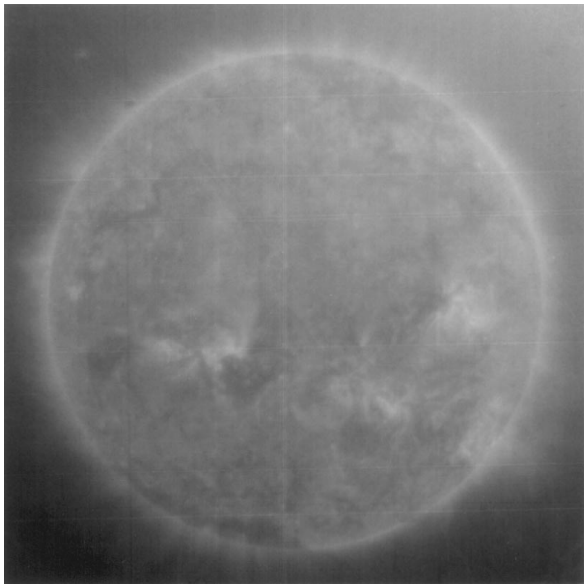

FIG. 7.—Corona in the 171–175 Å bandpass as observed in 1994. Solar north is rotated ~30° clockwise from the vertical.

cesses for the upper level i, and branching ratios to the lower level j). The function $K_n(T_e)$ represents the thermal response of the telescope. The function $a_H A_Z aZz(T_e)aZzij(T_e)\alpha_{Zzij}(Te)$ has been calculated by Mewe, Gronenschild, & van den Oord (1985) and by Landini & Fossi (1990). The telescope efficiency functions for the 1994 MSSTA flight have been measured by Kankelborg et al. (1995) and Plummer et al. (1995); Allen et al. (1993) and Lindblom et al. (1991) provide references to the calibration of the 1991 and 1987 flights. The normalized kernels, k_n [defined as $k_n(T)/k_n(T_n)$, where T_n is the temperature at which k_n is at its maximum value] for the MSSTA 171–175 Å, 171–190 Å, 190–205 Å, and 205–220 Å telescopes, derived from calibration data measured at the Stanford Synchrotron Radiation Laboratory, are given in Figure 12.

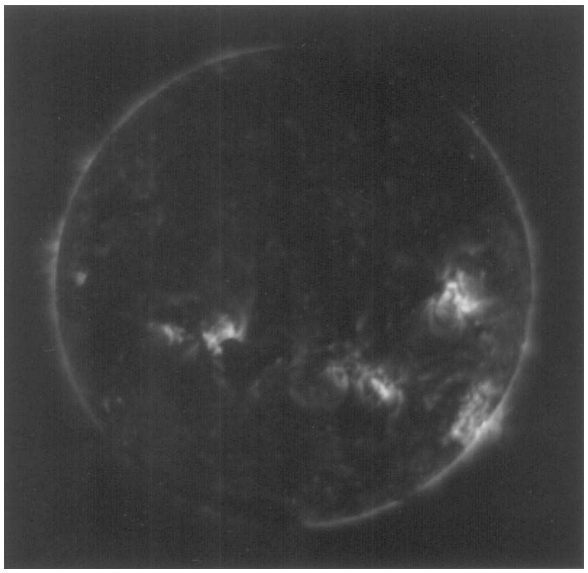

FIG. 8.—Corona as observed in the 284 Å bandpass in 1994. Solar north is rotated ~30° clockwise from the vertical.

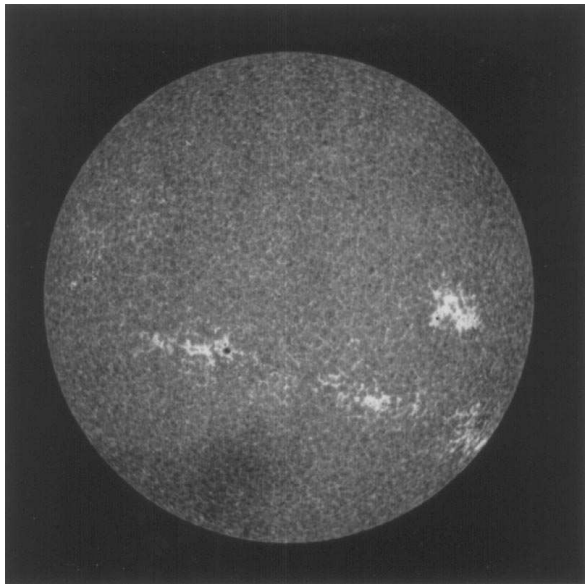

FIG. 9.—Solar disk in a bandpass centered on 1550 Å, which includes the 1600 Å continuum from the temperature minimum on the disk, the resonance lines of C IV, and lines of low-excitation ions such as Fe II and Si II. Solar north is rotated ~30° clockwise from the vertical.

3.2. *Photometry of the 1987 and 1994 Observations*

In order to determine the emission measure and temperature structure of the observed plasmas, we have performed a quantitative analysis on images digitized from the original flight negatives. Walker et al. (1993a) and Hoover et al. (1990c, 1992) have described the digitization and photometric calibration, respectively, of the flight film. The image was converted via film calibration from abstract pixel values to intensity units. The background was modeled by a flat-field average and subtracted from the original image.

For the 1987 171–175 Å image, average intensities measured in various regions on the solar disk (Fig. 13) in the bandpass from 171 to 175 Å are given in Table 1.

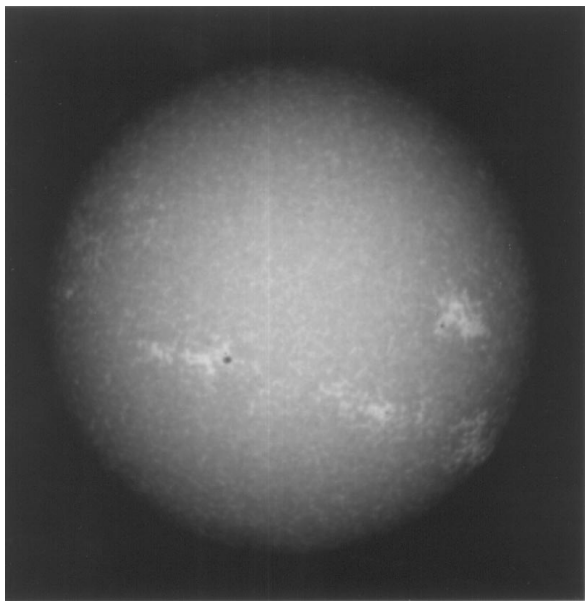

FIG. 10.—Lower transition region in H Lyα emission as observed in 1994. Solar north is rotated ~30° clockwise from the vertical.

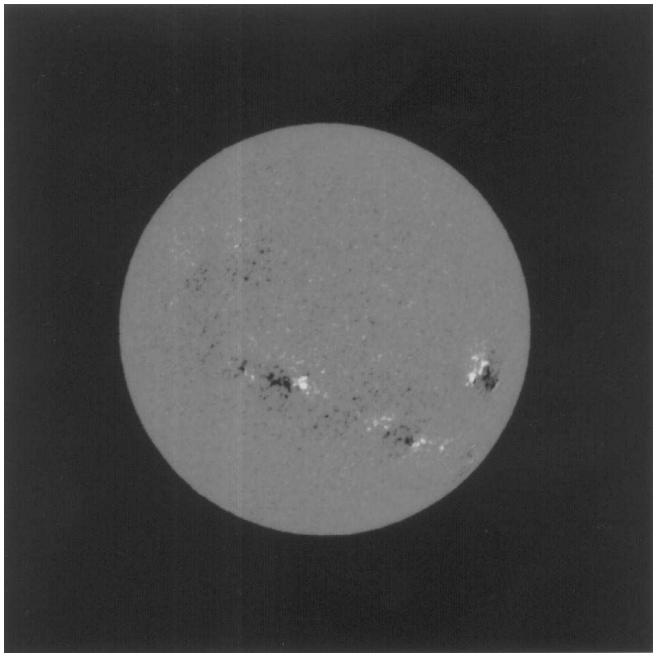

FIG. 11.—Kitt Peak magnetogram from 1994 November 4, the day after our flight. Solar north is rotated ~30° clockwise from the vertical.

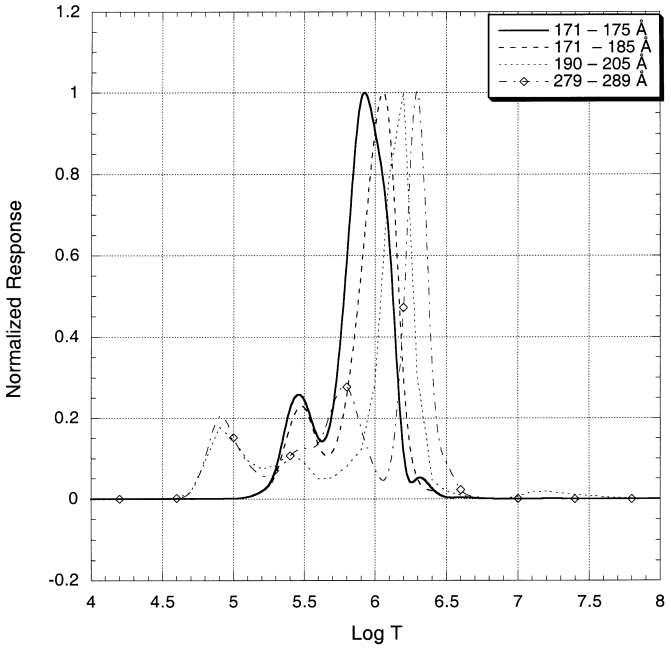

FIG. 12.—Responses of the 171–175 Å, 171–190 Å, 190–205 Å, and 279–289 Å telescopes to the solar plasma as a function of temperature. Each telescope has its primary temperature response in the upper transition region or lower corona; we note, however, that the 171–175 Å and 171–185 Å bandpasses respond to lines of O V and O VI in the temperature range of 200,000–400,000 K. The 190–205 Å bandpasses respond to lines of O V and He II excited at temperatures of 300,000 and 80,000 K, respectively. The 279–289 Å bandpass responds to Si VII and Mg VII emission, which each peak near 800,000 K; to Mg V, which is excited near 300,000 K; and to He II at 80,000 K.

3.3. *Temperature Estimation by Scale Height Analysis*

In the 1987 observations, we have one image in a bandpass (171–175 Å) corresponding to material in the corona and upper transition region. We obtained a second image in a bandpass centered at 256 Å (Walker et al. 1988) that is dominated by cooler material radiating in the He II Lyβ line. There are also strong lines of Fe XIV in this bandpass; thus, this image does not help constrain the temperature of the diffuse emission in the 171–175 Å image. In order to estimate the temperature of the plasma observed covering the disk in the 1987 171–175 Å image, we have analyzed the scale heights of structures at the limb. Four types of structures have been identified in various regions around the limb: active regions, plumes, interplume regions, and regions of quiet Sun (Fig. 13). Radial intensity profiles were extracted from the digitized image through each type of region, from the limb to the end of the observed emission. Figure 14 shows several of the flux curves that were generated.

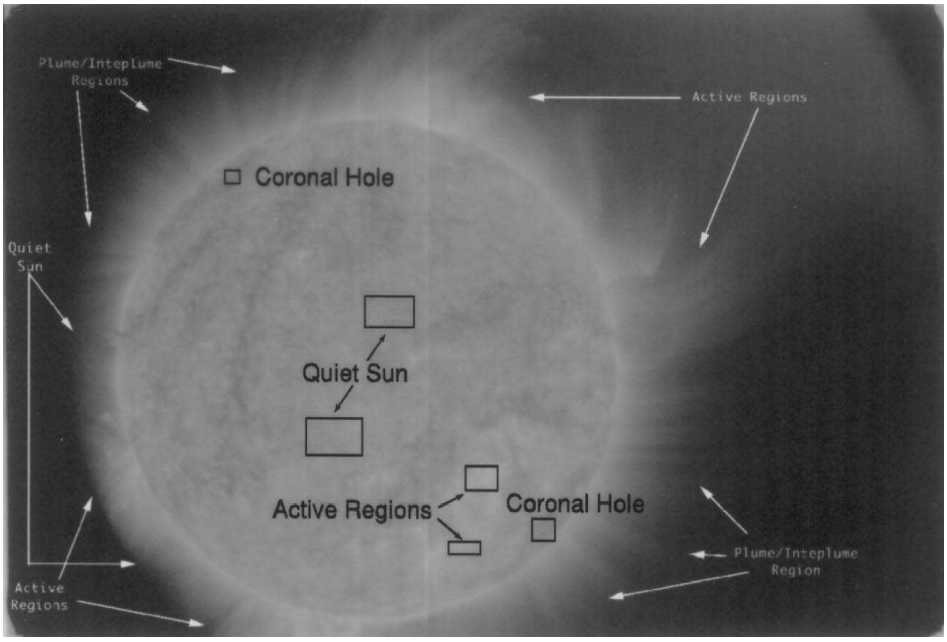

FIG. 13.—Regions on the solar disk and above the limb at which intensities were measured

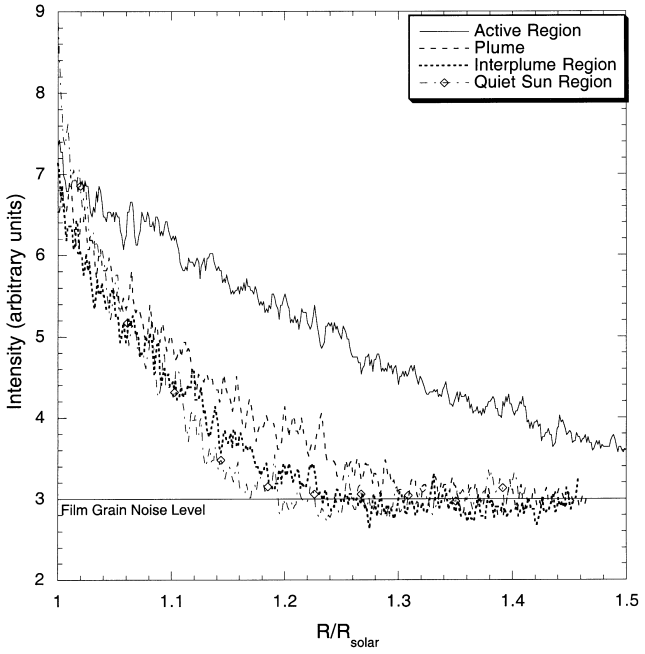

FIG. 14.—Measured EUV intensities at the film plane as a function of height above the center of the Sun through regions observed above the limb in our 1987 171–175 Å bandpass (Fe IX/X) image.

In a uniform gravitational field, the emission from an isothermal static plasma would fall exponentially with height. We have modeled the observed emission from each region with a static isothermal model. In hydrostatic equilibrium,

$$I(r) = I(r_0) \exp\left[\frac{2GM_\odot \mu m_H}{kT_e}\left(\frac{1}{r} - \frac{1}{r_0}\right)\right], \qquad (3)$$

where r is the radial distance form the solar center, m_H is the mass of a hydrogen atom, and μ is the mean molecular weight, which we take to be 0.61. Temperatures at several places around the limb derived from such fits are given in Table 2.

Although the intensities are observed to decrease exponentially with height, consistent with an isothermal, hydrostatic atmosphere, we nevertheless recognize the difficulties in deriving plasma temperatures from a scale-height analysis. Many physical processes that are likely to occur will cause departures from the isothermal and hydrostatic assumptions. Structures such as plumes and loops may contain flows and are magnetically contained. Furthermore, the line of sight through the optically thin plasma is unlikely to be isothermal. These conditions complicate the scale-height analysis, as previous authors have shown by comparing scale-height temperatures to temperatures derived by other means, such as line-ratio temperatures (Ahmad & Webb 1978; Falconer 1994). While noting these complications, the results presented in Table 2 nevertheless suggest that material in regions of quiet Sun not associated with plumes, loops, or other easily identified structures most likely has a temperature of $500{,}000 \leq T_e \leq 800{,}000$ K.

3.4. *Loop Model*

We model the structures responsible for the unresolved diffuse emission in Figures 2 and 4 as small loops.

3.4.1. *Physical Assumptions*

We assume that the plasma is confined in thin, symmetric loops with constant cross section, with maximum temperature T_m. Gravity is ignored and plasma flows are not taken into account. The model includes classical thermal conduction along the magnetic field and optically thin radiation in static energy balance with a constant energy input.

Since the emission we are concerned with originates from unresolved structures, we can use the spatial resolution of our telescope to constrain the geometries of the structures. We constrain the loops to be less than $\sim 10''$ in half-length, L, and choose a $1''.0$ diameter; we note that the thermal structure of the loops is not dependent on the loops' diameters. While the geometries chosen are similar to the lower transition region loops modeled by Antiochos & Noci (1986), the loop models we examine are hotter, $T_m >$ 250,000 K, and therefore, according to Cally & Robb (1991), stable. These models also differ from the "unresolved fine structure" model proposed by Feldman (1983) and recently examined by Spadaro, Lanza, & Antiochos (1996) by being hotter and by having an explicit "loop" geometry (see Dere et al. 1987). Our constant cross section assumption is consistent with the observations of previous authors (Klimchuk et al. 1992; O'Neal 1994). In fact, Zweibel & Boozer (1985) have pointed out that magnetic flux tubes with a small helical twist have a core field with constant cross section.

The work of FAL has shown that radiation in the H Lyα line is the principle sink for thermal energy conducted below 100,000 K. By including ambipolar diffusion in their models, they show that H Lyα emission is emitted from plasmas at temperatures (30,000–70,000 K) higher than the laboratory ionization equilibrium temperature of formation for H Lyα($\sim$20,000 K). They also show that ambipolar diffusion behaves as a heat sink, allowing the lower transition region to propagate particle heat fluxes in excess of the thermal conductive flux alone. In addition, Cally (1990) has shown that turbulent thermal conduction in the lower transition region may increase the emission from these plasmas

TABLE 1

SOLAR FLUXES IN THE 171–175 Å BANDPASS FOR VARIOUS CORONAL REGIONS

On-Disk Region	Film Plane Intensity (10^{-7} ergs s^{-1})	Film Plane Flux (10^{-1} ergs cm^{-2} s^{-1})	Solar Flux (10^{3} ergs cm^{-2} s^{-1})
Active Region I.....	4.46	3.16	5.85
Active Region II.....	3.88	2.75	5.08
Quiet Region I	1.69	1.20	2.21
Quiet Region II	1.93	1.37	2.52
Coronal Hole I.....	1.28	0.91	1.68
Coronal Hole II.....	1.16	0.82	1.52

by up to a factor of 3. Thus, we bound the temperatures, T_m, of our loop models at $T_0 = 100{,}000$ K at the footpoints of the loops, and assume that any energy conducted below this point will be radiated in lower transition region emission, primarily H Lyα. We assume loops that are symmetric in both their geometry and temperature structure, and place the position of maximum temperature in our loop models at the loop apex, consistent with the findings of previous authors (Durrant & Brown 1989; Klimchuck et al. 1992; Sturrock, Wheatland, & Acton 1996; Wheatland, Sturrock, & Acton 1997). This gives us a second boundary condition at the loop apex ($dT/dx = 0$).

3.4.2. *Model*

The principal quantities to be determined from the model are the conductive flux (which, evaluated at the loop base, is the energy available for lower transition region emission), temperature, and electron density as a function of position along the loop. From these quantities we can calculate the loop's EUV emission, which can be compared to our observations. We solve the one-dimensional loop equation for energy conservation and conduction,

$$\nabla \cdot \boldsymbol{F}_c = \frac{1}{A}\frac{d}{dx}(AF_c) = \epsilon - n_e^2 \Lambda(T) , \tag{4}$$

where $\boldsymbol{F}_c$ is the conductive thermal energy flux through a unit area along the loop, ϵ is the energy input per unit volume, $n_e^2 \Lambda(T)$ is the radiative energy loss per cubic centimeter, and A represents the cross-sectional area of the loop. We use the classical Spitzer conductivity for a fully ionized plasma,

$$F_c = -\kappa T^{-5/2}\frac{dT}{dx} , \tag{5}$$

where $\kappa \sim 10^{-6}$. The radiative loss function $\Lambda(T)$ (in ergs cm^3 s^{-1}) was fitted over power laws of the form $\Lambda(T) = \Lambda_s(T/T_s)^M$, and the values of the parameters Λ_s, T_s, and M are taken from Vesecky et al. (1979). Since we can neglect gravity because our loops are small compared to the gravitational scale height, our equation of state becomes

$$P = 2n_e kT = \text{constant} . \tag{6}$$

We are able to reduce the nonlinear second-order differential in equation (4) to first order, and write a definite-integral solution. Thus, the solution to equation (4) gives the temperature, density, and conductive flux along the loop. Using $T(x)$ and $n_e(x)$, we can employ our instrument response model described in § 3.1 to reproduce our observational results. A sketch of our adopted model geometry and energy balance is given in Figure 15.

3.4.3. *Computational Method*

To compute solutions for our loop model, we first choose our boundary condition at the base (T_0) of the loop, and find, for a particular choice of the parameters ϵ, n_{e0}, and F_{c0}, the position x along the loop where $dT/dx = 0$. Equation (4) is then integrated from the base of the loop, where $T = 100{,}000$ K, to the apex, where $dT/dx = 0$, using a fifth-order open Romberg method. The result is a determination of the loop half-length, L, the maximum temperature, T_m, and the temperature and density profiles of the loop. The model solutions were constrained by requiring the lengths of the loops to fall within our chosen size parameters, and requiring the loops' peak temperatures to lie within the upper transition region, $500{,}000 < T_e < 900{,}000$ K. We further constrained our models by requiring the energy loss due to thermal conduction to be equal to the loops' radiative losses.

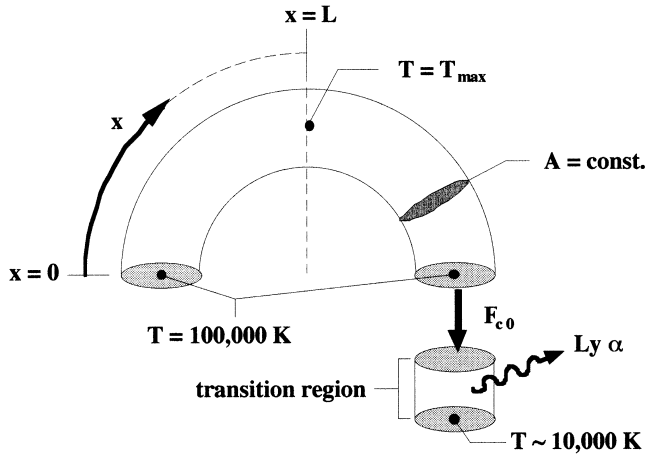

FIG. 15.—Sketch of the simple one-dimensional loop model used in this analysis.

4. RESULTS AND DISCUSSION

4.1. *Model Results*

Table 3 lists the peak temperatures, T_m, volumetric heating rates, ϵ, basal electron densities, n_{eo}, apex electron densities, n_{eL}, half-lengths, L, basal conductive heat fluxes, F_{c0}, radiative losses, F_R, and mechanical energy input flux, ϵL, for three representative loops. Three loops with maximum temperatures at $\sim$550,000 K (loop A), $\sim$750,000 K (loop B), and $\sim$ 900,000 K (loop C) are shown.

Figure 16 shows the temperature and density profiles for our representative loop models. We note that our choices for the input parameters n_{e0} and F_{c0} (which are predictions of the model) are not entirely arbitrary. The densities are constrained by observations of the solar transition region, which have generally found densities on the order of 10^9–10^{10} cm^{-3} for the quiet Sun and 10^{10}–10^{11} cm^{-3} for active regions (e.g., Bhatia & Thomas 1998; Doschek 1997; Cook, Brueckner, & Bartoe 1995; Raju & Gupta 1993; Malherbe et al. 1987; Woods 1986). Our choice of F_{c0}, $\sim 10^5$–10^6 ergs cm^{-2} s^{-1}, is consistent with observations of the solar area averaged H Lyα luminosity, which we equate with the basal conductive flux of our models (Allen et al. 1997; Kankel-

TABLE 2

TEMPERATURES DERIVED FROM SCALE-HEIGHT ANALYSIS THROUGH VARIOUS REGIONS ABOVE THE SOLAR LIMB

Limb Region	log T
Active Region I	6.19
Active Region II	6.19
Plume I	6.02
Plume II	5.95
Interplume Region I.....	5.82
Interplume Region II.....	5.82
Quit Sun Region I.....	5.80
Quiet Sun Region II	5.72

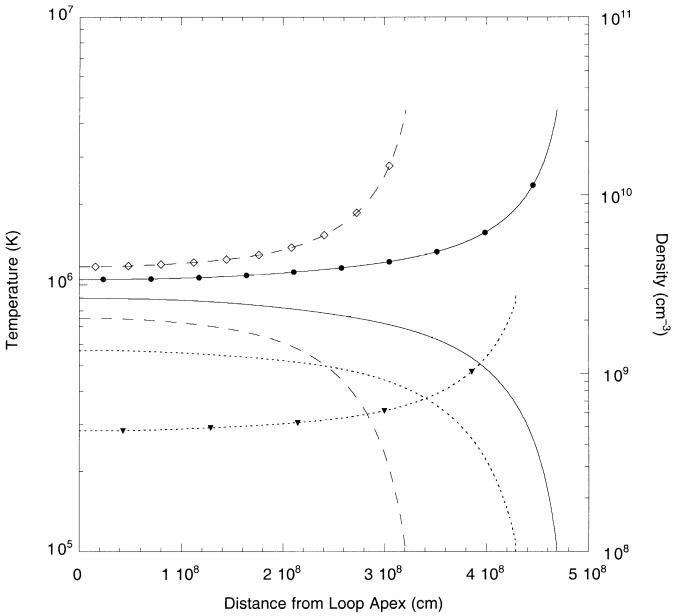

FIG. 16.—Temperature and density profiles calculated for representative loop models A, B, and C. Model A is represented by the solid lines, model B by the dashed lines, and model C by the dotted lines. The curves with markers show the density profiles for each respective model, and the unmarked curves show the temperature profiles.

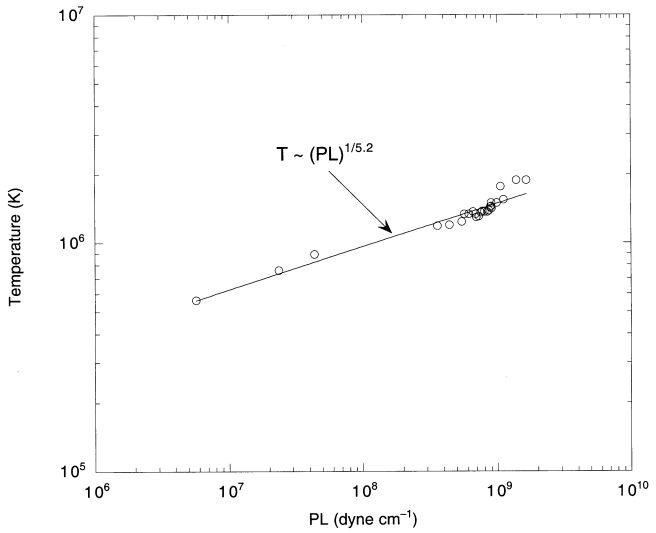

FIG. 17.—T vs. PL for our representative loop models, along with the 26 XBPs of Kankelborg et al. (1997).

borg et al. 1996, 1997) and with lower transition region models that include ambipolar diffusion (FAL).

4.2. *Comparison with Previous Observations*

Several previous observers have compared the results of their models and observations of coronal loops to the coronal loop scaling law of Rosner, Tucker, & Vaiana (1978; hereafter RTV; see also Garcia 1998; Kankelborg et al. 1997, 1996; Kano & Tsuneta 1996, 1995; Porter & Klimchuk 1995). The RTV scaling law, $T_m \propto (PL)^{1/3}$, relies on several assumptions. First, their boundary condition at the base of the loop is that the conductive flux vanish there. Second, they assume that radiation and the classical Spitzer conductivity are the only energy-loss mechanisms in the loop. Third, they assume that LTE conditions prevail from the corona down to the chromosphere. From these assumptions, they argue that radiative and conductive losses from the coronal portion of a loop are approximately equal for a loop in which gravity is negligible (i.e., less than a gravitational scale height). The work of FAL shows that none of these assumptions are strictly valid. Nevertheless, in this work we have constrained ourselves to consider only those models whose radiative losses are approximately equal to their conductive losses. In a later paper we will explore the solutions of the loop equation without the constraints of the RTV model. Figure 17 shows the results of plotting T_m versus PL for our representative models along with the results found for the 26 XBPs of Kankelborg et al. (1997, 1996). We see that our results are in approximate agreement with the results of Kankelborg et al. and extend the scaling-law relationship to cooler structures at subcoronal temperatures. We note, however, that systematic departures from and discrepancies with this scaling law have been found by several studies (Kankelborg et al. 1997, 1996; Kano & Tsuneta 1996, 1995; Porter & Klimchuk 1995; FAL; Roberts & Frankenthal 1980).

4.3. *Comparison with Spectral Observation*

We test our models by comparing them with emission-line observations. First we calculate the fluxes these models would produce in the bandpass of our 1987 173 Å telescope and compare it with the flux we measure in our image (see Table 2). This permits us to determine the number of loops that are necessary to explain our observations. We compare the number of loops required by our model with the number of network elements observed in our 1550 Å image. Next, we calculate temperature-diagnostic line ratios for Li-like ions excited most efficiently at upper transition region temperatures and compare them with previous observations. Finally, we calculate the absolute fluxes in several lines excited at upper transition region temperatures and compare them with measured fluxes. We believe that these three comparisons together provide a robust test of our models.

Using the Landini & Fossi (1990) line emissivity calculations, we have calculated the luminosities (ergs s^{-1}) that each model would produce in the six strongest lines in our bandpass for a 1″ cross section loop (see Table 4): Fe IX (171.07 Å), Fe X (174.51 Å), O V (172.17 Å), O VI (173.03 Å), Ne IV (172.60 Å), and Ne V (173.93 Å). Note that the models are calculated for a loop half-length, and hence the fluxes given are half the absolute flux from the total loop.

Using model B as an example, we calculate the disk coverage necessary to produce our observed emission. From Table 1 we see that the quiet-Sun flux in our

TABLE 3

MODEL RESULTS

Model Parameter	A	B	C
log T_m	5.75	5.88	5.95
ϵ (10^{-3} ergs cm^{-3} s^{-1})	1.22	8.46	6.87
n_{e0} (10^9 cm^{-3})	2.71	30.00	30.12
n_{eL} (10^9 cm^{-3})	0.48	3.99	3.38
L (10^8cm)	4.29	3.21	4.69
F_{c0} (10^5ergs cm^{-2} s^{-1})	2.74	9.00	11.67
F_R (10^5ergs cm^{-2} s^{-1})	2.48	18.16	20.53
$F_m = \epsilon L$ (10^5 ergs cm^{-2} s^{-1})	5.22	27.16	32.2

bandpass is measured to be ~ 2.0–2.5×10^3 ergs cm^{-2} s^{-1} at the Sun. From Table 4 we have calculated the emission in our bandpass that would be produced from model B to be 6.88×10^{19} ergs s^{-1}. Dividing by the maximum projected area of the loop (2.25×10^{16} cm^2) gives us 3.06×10^3 ergs cm^{-2} s^{-1}. The ratio of our measured flux, ~ 2.0–2.5×10^3 ergs cm^{-2} s^{-1}, and our calculated flux, 3.06×10^3 ergs cm^{-2} s^{-1}, implies that this model would match our observed data with $\sim$65%–80% disk coverage. This amount of coverage is in good agreement with the observed coverage in our 1987 171–175 Å image. Using this amount of coverage, we can calculate the area on the solar disk that these loops must cover. Dividing this number by the projected area of a single loop gives us the number of loops required to cover this fraction of the solar disk. Table 5 summarizes the data for each of our representative models.

From Table 5 we see that models B and C with $700{,}000 \leq T_m \leq 900{,}000$ K can yield good matches to our observed data with reasonable disk coverages. We note that because of the limited spatial resolution of our instrument, unresolved structures would be smeared; thus, a range of coverages may constitute an acceptable model until observations with better spatial resolution are available. Consequently, the parameters of our model, which include the electron densities and cross sections of the loops, are not strongly constrained. Hence, the number of loops required to satisfy our observed intensity is not strongly constrained, except by the number of network elements observed in lower transition region lines such as C IV and H Lyα. We have performed a count of the number of network elements in a unit area observed in our 1994 1550 Å image and extrapolated this number to the number of elements that should be on the entire solar disk. The total number of network elements inferred is approximately 25,000–50,000. We see that the models that we have calculated assuming a 1″ loop cross section predict on the order of 100,000 loops to satisfy our observations. Since the cross sections we have chosen are somewhat arbitrary, we can decrease the number of loops required by increasing the loops' cross sections, which increases their volumes and hence their emission measures. For example, if we double the cross-sectional area of our loops to 2″, we quadruple the loops' luminosities and double their projected areas. Consequently, a smaller number of loops would be required to satisfy our observations. On the other hand, the number of loops that we calculate to satisfy our observations may very well be consistent with the number of network elements that we count if we do not assume that each loop has a unique set of footpoints. High-resolution observations by the *TRACE* satellite have revealed that what at lower resolution appear to be single loops may be resolved into several individual loops sharing common footpoints. In order to make our models consistent with both our EUV (at 173 Å) and FUV (at 1550 Å) observations, it would be necessary to resolve the structures in each regime. Nevertheless, we conclude that the number of loops that we calculate from our EUV observations is not incompatible or inconsistent with the number of network elements we count in our FUV image.

To further test the assumption that the small "lukewarm" loops of the types modeled here create the bulk of the quiet-Sun emission for lines formed in the upper transition region, we compare temperature-sensitive diagnostic line ratios predicted by our models to those measured by previous experimenters. The ratio of the $2s\ S^2$–$2p\ P^2$ transition lines (1031.95 and 1037.65 Å) of the Li-like O VI ion to the $2s\ S^2$–$3p\ P^2$ (150.1 Å) and $2p\ P^2$–$3d\ D^2$ transition lines at 173.03 Å of O VI varies strongly with temperature (Walker 1975). Since the models that we present here represent a nonisothermal plasma with a distribution of temperatures and the set of all loop models forms a continuous set, whereas the set of models that would give us the proper diagnostic line ratio is a discrete set, these diagnostic line ratios provide a good test of our models. We are in the process of calculating line intensities for several of the models we have derived. We present preliminary results of temperature diagnostic line ratios of the 1031.95, 1037.65, and 150.1 Å lines to the 173.03 Å line of O VI. Table 6 gives the comparisons. The values given in the table represent the ratios of the line ratios calculated from our representative loop models to the ratio as measured by Malinovsky & Heroux (1973). Figure 18 shows the values of our calculated ratios for our models and the measured ratio of Malinovsky & Heroux superimposed on the curve representing the ratio of the emission profile of the 1031.95 Å

TABLE 4

LINE EMISSION FOR LOOP MODELS

Model	Fe IX (ergs s^{-1})	Fe X (ergs s^{-1})	O V (ergs s^{-1})	O VI (ergs s^{-1})	Ne IV (ergs s^{-1})	Ne V (ergs s^{-1})	Total (ergs s^{-1})
A.....	3.50×10^{17}	1.51×10^{16}	1.96×10^{17}	2.94×10^{17}	7.81×10^{16}	2.30×10^{16}	9.57×10^{17}
B.....	4.63×10^{19}	7.31×10^{18}	5.57×10^{18}	6.88×10^{18}	2.23×10^{18}	4.68×10^{17}	6.88×10^{19}
C.....	1.87×10^{20}	4.97×10^{19}	1.17×10^{19}	1.51×10^{19}	4.65×10^{18}	9.81×10^{17}	2.69×10^{20}

TABLE 5

DISK COVERAGE AND NUMBER OF LOOPS

Model	Log T_m	Solar Bandpass Luminosity (ergs cm^2 s^{-1})	Coverage (%)	Corresponding Area on Solar Disk (10^{22} cm^2)	Number of Loops Necessary ($\times 10^5$)
A.....	5.75	3.19×10^1	$\geqslant 100$	$\geqslant 1.5$	>2.5
B.....	5.88	3.06×10^3	65–80	1.0	2.22
C.....	5.95	8.61×10^3	25–30	0.4	0.61

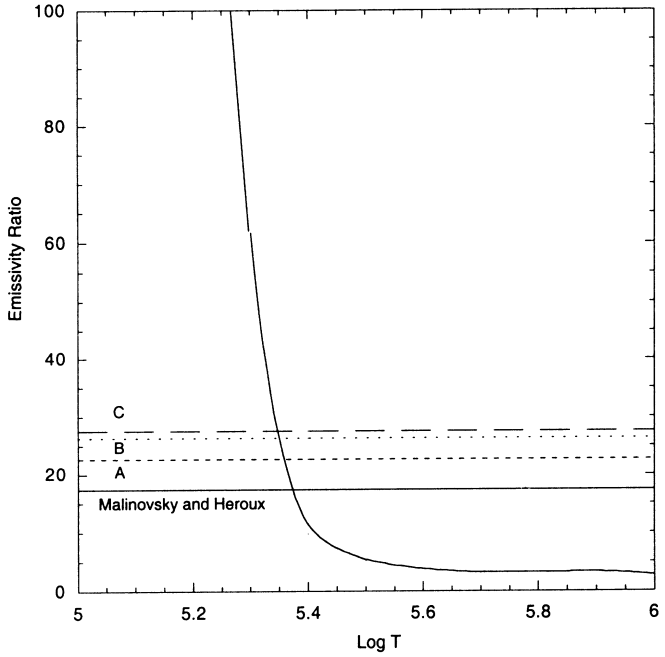

FIG. 18.—Ratio of the emissivity functions of the Li-like ions of O VI at 1032 and 173.03 Å. Horizontal lines indicate the values of the ratios derived from our models.

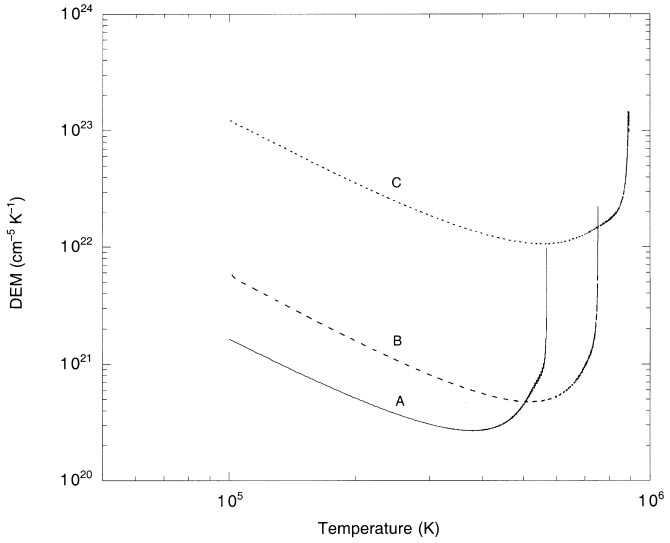

FIG. 19.—Differential emission measure curves derived for models A, B, and C.

line to the 173.03 Å line. Referring to Table 6, we note that our models overestimate the value of the ratio of the 1031.95 and 1037.65 Å line to the 173.03 Å line. This result is not unexpected. The Malinovsky & Heroux (1973) measurements are full-disk fluxes. The presence of elevated temperatures and densities of active regions on the disk would tend to decrease the ratio of the 1031.95 and 1037.65 Å lines to the 173.03 Å line. We conclude then that the ratios calculated from our models are in rough agreement with the measured ratio of Malinovsky & Heroux.

We can explore the effect of active regions on the full-disk fluxes mentioned above by comparing the absolute flux from the cooler emission lines of O VI at 1031.95 and 1037.65 Å. Table 7 gives the fluxes calculated for the emission lines of O VI at 1031.95 and 1037.65 Å from our models and the fluxes as measured by Malinovsky & Heroux (1973). We note that the Malinovsky & Heroux measurements were made on 1969 April 4, which was near solar maximum, while our measurements were made on 1987 October 23, near solar minimum. Rugge & Walker (1970) showed that the 2800 MHz solar flux is an excellent proxy for the solar EUV for X-ray fluxes. By comparing the 2800 MHz flux for the date of the Malinovsky & Heroux flight (177.3) to the flux on the date of our flight (87.0), we can normalize the Malinovsky & Heroux flux to the date of our flight so as to correspond to the difference in the solar cycle. When this correction is made, reasonable agreement is found between our calculated fluxes and the measured fluxes of Malinovsky & Heroux, suggesting that our models are consistent with the hypothesis that the quiet-Sun emission in lines emitted in this temperature range is dominated by lukewarm loops with peak temperatures in the range 500,000–900,000 K.

Figure 19 shows the differential emission measure as a function of temperature for our representative models. Table 8 gives the relative contributions each ion makes to the total bandpass luminosity. We see that ~10%–50% of the emission in the 171–175 Å bandpass may come from the cooler lines of O V, O VI, Ne IV, and Ne V for the lukewarm loop models. This is a significant contribution. For comparison, consider that we have measured the total emission due to active regions above the limb and on the disk to account for ~25% of the total emission in this image, taken near solar minimum. Thus, interpreting the emission from a multilayer bandpass (such as the 171–175 Å bandpass used on the MSSTA, EIT, and *TRACE*) as representing million-degree plasma is a naive assumption without detailed modeling of a structure's emission profile. We also note that ~75% of the emission in this bandpass, centered on Fe IX

TABLE 6

COMPARISON OF CALCULATED TEMPERATURE-SENSITIVE DIAGNOSTIC LINE RATIOS FOR O VI TO THE MEASUREMENTS OF MALINOVSKY & HEROUX NORMALIZED TO THE 173.3 Å LINE

Model	1037.65 Å	1031.95 Å	173.10 Å	150.10 Å
M&H.....	8.13	17.43	1.00	0.83
A.....	11.73	22.63	1.00	0.55
B.....	14.33	27.60	1.00	0.56
C.....	13.68	26.37	1.00	0.55

TABLE 7

COMPARISON OF CALCULATED ABSOLUTE FLUXES OF O VI EMISSION LINES TO THE MEASUREMENTS OF MALINOVSKY & HEROUX

Model	O VI 1038 Å Flux (10^{-3} ergs cm^{-2} s^{-1})	O VI 1032 Å Flux ($\times 10^{-3}$ ergs cm^{-2} s^{-1})
M&H	24.4	52.3
M&H corrected.....	11.97	25.66
A	0.30	0.58
B	10.47	20.16
C	4.95	9.55

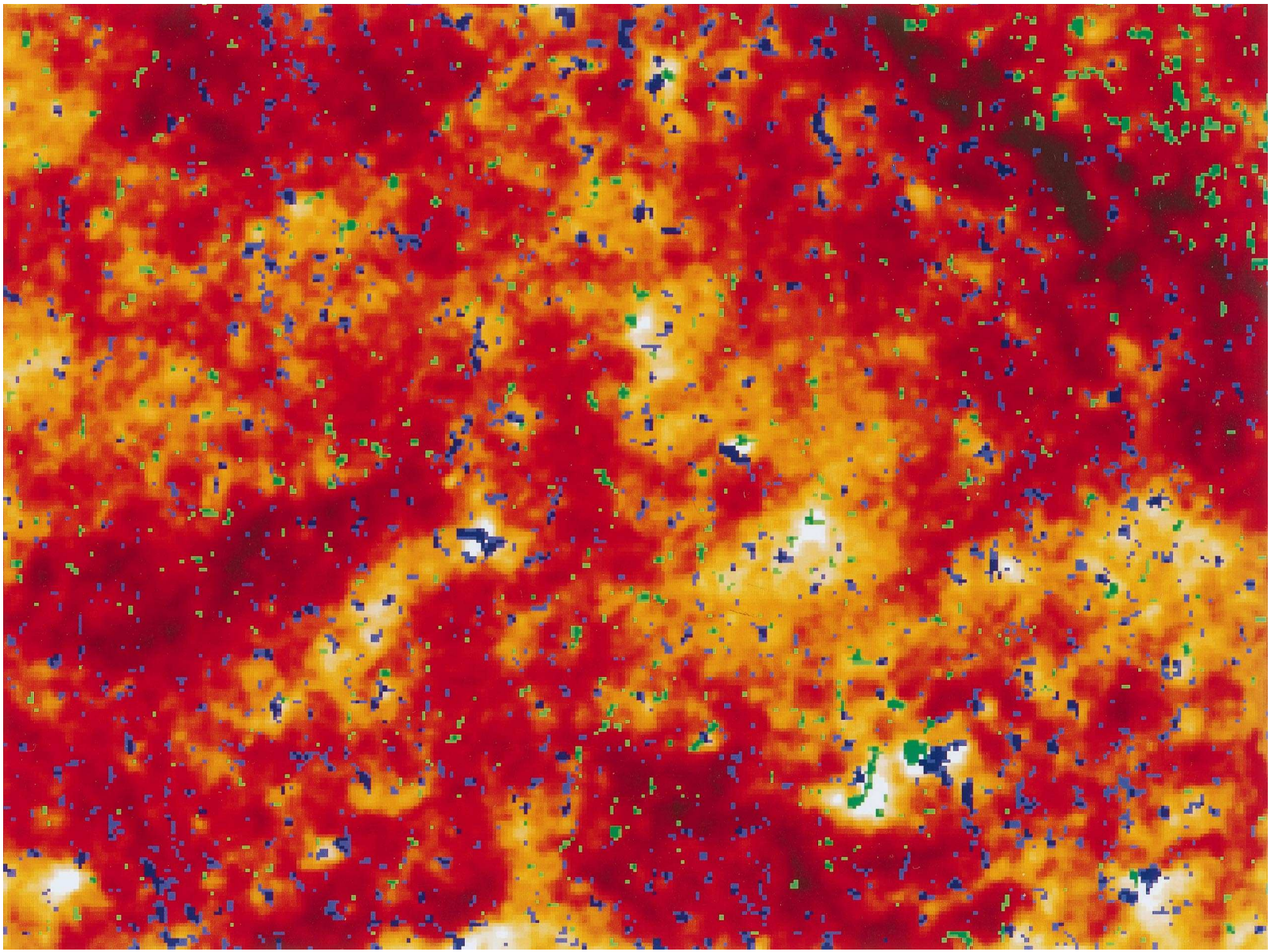

FIG. 20.—Central portion of the 171–175 Å image from the 1987 flight, spanning about 1 solar radius from top to bottom and about $1\frac{1}{3}$ solar radius from side to side. The EUV image, obtained at UT 18:09 on 1987 October 23, is shown in the red-white color scale. Superimposed on this are photospheric magnetic flux concentrations, from the Kitt Peak magnetogram taken that day (beginning at UT 17:25 and continuing for about 1 hr). Positive flux is shown in blue and negative flux is shown in green. The darker shades correspond to field strengths of 30 G or more (pixels were binned to 4″ resolution). The lighter shades represent field strengths of 14–29 G.

(which radiates most strongly at 10^6 K), arises not from active regions but from the quiet Sun. This indicates that at solar minimum there is enough material present with $\sim 500{,}000 \leq T_e < 900{,}000$ K for the Fe IX emission from these plasmas to dominate the Fe IX emission from the hotter active region plasmas, despite the fact that Fe IX is emitted less efficiently at these cooler temperatures.

We recognize that these results do not conclusively demonstrate that the unresolved structures responsible for the quiet-Sun emission in our 1987 170–175 Å image originate from the lukewarm loops we postulate, or that the structures are loops at all; we can say, however, that we have illustrated that solutions exist for the models presented here that are consistent with our observations.

4.4. *Association with the Network*

Our model of the structures that generate the EUV emission observed by our 171–175 Å bandpass telescope postulates a number of small loops with a projected area of ~ 20 arcsec^2 or less each. These loops must have footpoints in the network, which raises the question of whether there is evidence for the existence of such loops in chromospheric and lower transition region images and in magnetograms. We begin this discussion by noting that our models are reasonably well constrained in temperature by our observations, but are constrained in density only by a relatively small number of observations (from other observers) that utilize density-sensitive line ratios to study material at transition-region temperatures. This material may or may not correspond to the structures that we have modeled (see, e.g., Doschek et al. 1998). Since the luminosity of a loop varies as the square of density, the predicted fractional coverage of the solar surface by the loops we model is also not strongly constrained. Although our images suggest that more than 50% of the solar surface is covered by structures that radiate in the 171–175 Å bandpass, if the structures responsible for this emission have at least one dimension that is smaller than the resolution of our images, then the coverage of the solar surface may well be smaller than 50%. The number of loops necessary to generate the flux levels we observe is on the order of 100,000 loops (see Table 5). In our previous studies of polar plumes and XBPs (Allen et al. 1997; Kankelborg et al. 1996, 1997), we were able to relate coronal structures to the local network structures at their bases as observed in H Lyα. Unfortunately, we do not have an FUV image of lower transition region or chromospheric material from our 1987 flight. We do, however, have a magnetogram image corresponding to the time of our flight.

Figure 20 shows the central portion of the 171–175 Å image from the 1987 flight, spanning about 1 solar radius from top to bottom and about $1\frac{1}{3}$ solar radius from side to side (solar north is up). The EUV network is partially masked in some areas by bright larger-scale diffuse emission, but over most of the large area shown, there is a clear correspondence between the magnetic network and enhanced emission in the 171–175 Å bandpass. (Note that some care must be taken in comparing magnetic and emission features near the edges of the image, since projection effects shift the EUV features limbward of their photospheric counterparts.) The magnetic flux concentrations are scattered along bright rings of EUV emission, so that most of them are embedded in bright halos of emission. The emission enhancements are generally strongest over the strongest bipoles. Owing to the 14 G cutoff and 4″ pixel binning in the magnetogram, many more bipoles must be present than are revealed by this image. As Wang & Sheeley (1995) note, even when the network field configuration appears to be unipolar on the scales probed by the Kitt Peak National Observatory magnetograms, there is evidence that bipolar structures exists on scales of a few arcseconds. These small-scale magnetic bipoles may provide one possible explanation for the larger scale diffuse emission that exists in the interiors of the network cells. Small dynamic loops overlaying small-scale magnetic bipoles emerging in cell centers, consistent with the "magnetic carpet" model of Schrijver et al. (1997), could produce the diffuse emission of the cell centers seen in Figure 19. We note that other possible explanations for the diffuse emission of the cell centers include funnels of the type postulated by Gabriel (1976) and long low-density loops crossing several cells (C. J. Schrijver 1997, private communication). Previous authors have also pointed out the spatial correspondence between the magnetic network and the network as observed in the chromosphere and transition region (Dowdy 1993; Athay 1981a). It follows then that the emission we have observed, which we postulate originates from lukewarm loops, corresponds spatially with the network.

Observations of the lower transition region network show thousands of discrete network structures that are $\sim 5''$–$10''$ or less in size. One interpretation of the nature of these structures, observed for example by the *SOHO* SUMER experiment at 1406 Å (S VI) and 937.8 (H Lyϵ) (Lemaire et al. 1997), and by the *SOHO* CDS experiment at 584.33 Å (He I), 303.78 Å (He II), 525.80 Å (O III), 554.51 Å (O IV), 629.73 Å (O V), 562.8 Å (Ne VI), 313.74 Å (Mg VII), 319.83 Å (Si VIII), 368.07 Å (Mg IX), and 624.95 Å (Mg X) (Gallagher et al. 1998) and by the MSSTA in bands that include 1550 Å (C IV) and 1216 Å (H Lyα), is that they are the footpoints of magnetic flux tubes connected to hotter material. If this interpretation is correct, these network elements could well be the footpoints of the "lukewarm" loops that we have postulated as the source of the quiet-Sun EUV

TABLE 8

RELATIVE PERCENTAGES OF LINE EMISSION TO TOTAL BANDPASS LUMINOSITY

Model	log T_m (K)	Fe IX (171.07 Å)	Fe X (174.51 Å)	O V (172.17 Å)	O VI (173.03 Å)	Ne IV (172.60 Å)	Ne V (173.93 Å)
Bandpass throughput normalized to peak response.....		1	0.385	0.808	0.615	0.615	0.538
A	5.75	46	1	21	24	6	2
B	5.88	78	5	8	7	2	0.4
C	5.95	82	8	4	4	1	0.2

radiation. We note that the network pattern is visible, with little change, in lines formed at temperatures up to $\sim$800,000 K (Gallagher et al. 1998). At coronal temperatures, however, the network pattern begins to disappear and only the bright coronal structures are visible. This would seem to indicate, as Dowdy (1993) has pointed out, that there are structures in the network that never reach coronal temperatures. These subcoronal structures could very well be the lukewarm loops we postulate. This point highlights one difference between the model of Gabriel (1976) and the model assumed in our analysis. Gabriel's model appears to require that network plasma is always associated with the plasmas at coronal temperatures; in our model, the network plasmas are only associated with coronal plasmas if larger, hotter loops, XBPs, or polar plumes are present. Gabriel assumes that large areas of the network are unipolar, and that flux tubes in the network are not twisted helically. There is evidence that, at least in the quiet network, neither assumption is strictly true. Our model appears to best explain observations taken near solar minimum. At solar maximum, the increased presence of hotter active-region loop systems may obscure the "transition region" plasmas associated with the network. In the next section, we ask the question, "what is the relationship between our lukewarm loops and the emission generated in lines formed at lower transition region temperatures?"

4.5. *Heating of the Lower Transition Region*

It is interesting to calculate the energy available for lower transition emission from our models. The total radiative flux from the lower transition region, including H Lyα, is observed to be 5×10^5 ergs cm^{-2} s^{-1} (Timothy 1977; Vidal-Madjar 1977). Athay (1985) estimates the conductive energy flux parallel to magnetic field lines between 10^5 and 10^6 K to be $\sim 1 \times 10^6$ ergs cm^{-2} s^{-1}. Using the conductive flux values from Table 3, the calculated disk coverages from Table 5, and correcting for active regions, we find that model B would conduct $\sim 6 \times 10^5$ ergs cm^{-2} s^{-1} into the lower transition region. These conductive flux levels are consistent with the total heat fluxes at 100,000 K derived by FAL in their lower transition region models, which include ambipolar diffusion. Previous lower transition region models, which did not include ambipolar diffusion, predicted substantially lower heat fluxes, leading to the conclusion that lower transition region emission could not be generated by conduction from hotter plasmas (presumably coronal plasmas). While our results do not exclude the possibility of other energy sources for lower transition region emission, they do suggest a significant role for conduction from plasmas at subcoronal temperatures. The lukewarm loops could provide, then, a significant fraction of the energy radiated as quiet-Sun lower transition region emission in the local lower transition network at their footpoints.

4.6. *Chromospheric Interface*

Ayres & Rabin (1996) have suggested that the chromosphere is only present in magnetic flux tubes, and that the chromosphere typically covers $\sim$20% of the solar surface. Their model is based on infrared observations that indicate that material cooler than the temperature minimum, associated with emission due to the CO molecule, is present over most of the solar surface. The chromosphere, in their model, is associated only with plasma in magnetic flux tubes. At least some of the plasma at chromospheric temperatures 4000–20,000 K, if we wish to associate chromospheric emission with the Ca I and Mg II emission (see Vernazza, Avrett, & Loeser 1983), must be at the footpoints of the lukewarm flux tubes that we have modeled.

4.7. *Conclusions*

We have presented evidence that the unresolved structures responsible for much of the quiet-Sun emission in our 1987 and 1994 171–175 Å images are at subcoronal temperatures ($T < 10^6$ K). This is an important conclusion, since it directly impacts the interpretation of the temperature structure of features imaged with multilayer optics. We have calculated the flux our models would produce in the bandpass of our 173 Å 1987 telescope. Loop models with peak temperatures between 700,000 and 900,000 K match the observational data well. A preliminary comparison of Li-like O VI emission-line ratios calculated from our loop models agree well with the measured ratio of Malinovsky & Heroux (1973). The absolute fluxes in typical FUV upper transition region lines have also been calculated from our models and compared with observations; good agreement is found. Our energy balance calculations also indicate that the lukewarm loops that we model may impart enough energy through classical thermal conduction into the lower transition region to account for a significant fraction of the quiet-Sun lower transition region emission. We have pointed out previously (Allen et al. 1997; Kankelborg et al. 1996, 1997) that the chromosphere/corona interface at the footpoints of polar plumes and XBPs may make a significant, perhaps dominant, contribution to the energy emitted by the local network in the lower transition region, contrary to the views expressed by a number of authors. In the present paper we show that it is possible that the interface between structures at subcoronal temperatures and the chromosphere can make a significant contribution to the energy emitted by the local lower transition region network in the quiet Sun.

This research was supported by NASA grant NSG-5131 at Stanford and NASA/MSFC; Troy W. Barbee, Jr. was supported by DOE contract W-7405-Eng-48. We wish to thank the team at the Stanford Synchrotron Radiation Laboratory and the SURF-II team at National Institute for Standards and Technology for their assistance during calibration measurements at their respective laboratories. The authors would like to thank Ron Moore of NASA/MSFC for discussions of the correspondence of the EUV and magnetic networks, David Santiago of Stanford University and Charles Kankelborg of Montana State University for discussions of our numerical models, and Paul Boerner of Stanford University for numerous enlightening conversations. We would like to thank David Falconer of NASA/MSFC for help with the presentation of Figure 19 and Mark Vande Hei and Carmel Levitan of Stanford University for help with the presentation of Figure 17 and Table 6. We are extremely grateful to NSO/Kitt Peak for the magnetograms used in Figures 1 (*right*), 2*c*, 11, and 20.

REFERENCES

Ahmad, I. A., & Webb, D. F. 1978, Sol. Phys., 58, 323
Allen, M. J., Oluseyi, H. M., Walker, A. B. C., II, Hoover, R. B., & Barbee, T. W. 1997, Sol. Phys, 174, 367
Allen, M. J., Willis, T. D., Kankelborg, C. C., O'Neal, R. H., Martinez-Galarce, D. S., DeForest, C. E., Jackson, L. R., Plummer, J. E., & Walker, A. B. C. 1993, Proc. SPIE, 2011, 381
Antiochos, S. K., & Noci, G. 1986, ApJ, 301, 440
Athay, R. G. 1981a, ApJ, 249, 340
———. 1981b, ApJ, 250, 709
———. 1984, ApJ, 287, 412
———. 1985, Sol. Phys., 100, 257
Ayres, T. R., & Rabin, D. 1996, ApJ, 460, 1042
Barbee, T. W., Jr. 1990, Opt. Eng., 29, 711
Berger, T. E., Lofdahl, M. G., Shine, R. S., & Title, A. M. 1998, ApJ, 495, 973
Berger, T. E., Shine, R. S., Title, A. M., Tarbull, T. D., & Sharmer, G. 1995, ApJ, 454, 531
Berger, T. E., & Title, A. M. 1996, ApJ, 463, 365
Bhatia, A. K., & Thomas, R. J. 1998, ApJ, 497, 483
Cally, P. S. 1990, ApJ, 355, 693
Cally, P. S., & Robb, T. D. 1991, ApJ, 372, 329
Cook, J. W., Keenan, F. P., Dufton, P. L., Kingston, A. E., Pradhan, A. K., Zhang, H. L., Doyle, J. G., & Hayes, M. A. 1995, ApJ, 444, 936
DeForest, C. E., et al. 1991, Opt. Eng., 30, 1125
Dere, K. P., Bartoe, J. F., Brueckner, G. E., Cook, J. W., & Socker, D. G. 1987, Science, 238, 1267
Doschek, G. A. 1997, ApJ, 476, 730
Doschek, G. A., Laming, J. M., Feldman, U., Wilhelm, K., Lemaire, P., Schüle, U., & Hassler, D. M. 1998, ApJ, 504, 573
Dowdy, J. F. 1993, ApJ, 411, 406
Dowdy, J. F., Emslie, A. G., & Moore, R. L. 1987, Sol. Phys., 112, 255
Dowdy, J. F., Rabin, D., & Moore, R. L. 1986, Sol. Phys., 105, 35
Durrant, C. J., & Brown, S. F. 1989, Proc. Astron. Soc. Australia, 8, 137
Falconer, D. A. 1994, NASA Tech. Mem. 104616 (Washington: NASA)
Falconer, D. A., Moore, R. L., Porter, J. G., Gary, G. A., & Shimizu, T. 1996, ApJ, 482, 519
Falconer, D. A., Moore, R. L., Porter, J. G., & Hathaway, D. H. 1998, ApJ, 501, 386
Feldman, U. 1983, ApJ, 275, 367
———. 1987, ApJ, 320, 426
Fludra, A., Brekke, P., Harrison, R. A., Mason, H. E., Pike, C. D., Thompson, W. T., & Young, P. R. 1997, Sol. Phys., 175, 487
Fontenla, J. M., Avrett, E. H., & Loeser, R. 1990, ApJ, 355, 700
———. 1991, ApJ, 377, 712
———. 1993, ApJ, 406, 319
Gabriel, A. H. 1976, Philos. Trans. R. Soc. London, A281, 339
Gallagher, P. T., Phillips, K. J. H., Harra-Murnion, L. K., & Keenan, F. P. 1998, A&A, 335, 733
Garcia, H. A. 1998, ApJ, 504, 1051
Giovanelli, R. G. 1949, MNRAS, 109, 372
Golub, L. 1980, Philos. Trans. R. Soc. London, A297, 595
Hoover, R. B., Barbee, T. W., Walker, A. B. C., Lindblom, J. F., O'Neal, R. H., & Baker, P. C. 1990a, Opt. Eng., 29, 1281
Hoover, R. B., et al. 1990b, Proc. SPIE, 1343, 189
Hoover, R. B., Walker, A. B. C., DeForest, C. E., Allen, M. J., Lindblom, J. F., O'Neal, R. H., Paris, E. S., & DeWan, A. 1990c, Proc. SPIE, 1343, 175
Hoover, R. B., Walker, A. B. C., DeForest, C. E., Watts, R. N., & Tarrio, C. 1992, Proc. SPIE, 1742, 549
Kankelborg, C. C., et al. 1995, Proc. SPIE, 2515, 436
Kankelborg C. C., Walker, A. B. C., & Hoover, R. B. 1997, ApJ, 491, 952
Kankelborg, C. C., Walker, A. B. C., Hoover, R. B., & Barbee, T. W. 1996, ApJ, 466, 529
Kano, R., & Tsuneta, S. 1995, ApJ, 454, 934
———. 1996, Publ. Astron. Soc. Japan, 48, 535
Klimchuk, J. A., Lemen, J. R., Feldman, U., Tsuneta, S., & Uchida, Y. 1992, PASJ, 44, L181
Landini, M., & Fossi, B. C. 1990, A&AS, 82, 229
Lemaire, P., et al. 1997, Sol. Phys., 170, 105
Lindblom, J., O'Neal, R. H., Walker, A. B. C., Powell, F. R., Barbee, T. W., Hoover, R. B., & Powell, S. 1991, Proc. SPIE, 1343, 544
Malherbe, J. M., Schmieder, B., Simon, G., Mein, P., & Mein, P. 1987, Sol. Phys., 112, 233
Malinovsky, M., & Heroux, M. 1973, ApJ, 181, 1009
Martínez-Galarce, D. S., Walker, A. B. C., II, Gore, D. B., Kankelborg, C. C., Hoover, R. B., & Barbee, T. W. 1998, Opt. Eng., submitted
Mewe, R., Gronenschild, E. H. B. M., & van den Oord, G. H. J. 1985, A&AS, 62, 197
Oluseyi, H. M., & Walker, A. B. C., II. 1999, in preparation
O'Neal, R. H. 1994, Ph.D. thesis, Stanford University
Plummer, J. E., et al. 1995, Proc SPIE, 2515, 565
Porter, L. J., & Klimchuk, J. A. 1995, ApJ, 454, 499
Pres, P., & Phillips, K. 1999, ApJ, 510, L73
Rabin, D. 1991, ApJ, 383, 407
Rabin, D., & Moore, R. 1984, ApJ, 285, 359
Raju, P. K., & Gupta, A. K. 1993, Sol. Phys., 145, 241
Reeves, E. M. 1976, Sol. Phys., 46, 53
Reeves, E. M., Huber, M. C. E., & Timothy, J. G. 1977, Appl. Optics, 16, 837
Reeves, E. M., Vernazza, J. E., & Withbroe, G. L. 1976, Philos. Trans. R. Soc. London, A281, 319
Roberts, B., & Frankenthal, S. 1980, Sol. Phys., 68, 103
Rosner, R., Tucker, W. H., & Vaiana, G. S. 1978, ApJ, 220, 643 (RTV)
Rugge, H. R., & Walker, A. B. C. 1970, Sol. Phys., 15, 372
Schrijver, C. J., Title, A. M., Van Ballegooijen, A. A., Hagenaar, H. J., & Shine, R. A. 1997, ApJ, 487, 424
Spadaro, D., Lanza, A. F., & Antiochos, S. K. 1996, ApJ, 462, 1011
Sturrock, P. A., Wheatland, M. S., & Acton, L. W. 1996, ApJ, 461, L115
Timothy, J. G. 1977, in The Solar Ouput and Its Variations, ed. O. R. White (Boulder: Univ. Colorado), 237
Vernazza, J. E., Avrett, E. H., & Loeser, R. 1981, ApJS, 45, 635
Vesecky, J. F., Antiochos, S. K., & Underwood, J. H. 1979, ApJ, 233, 987
Vidal-Madjar, A. 1977, in The Solar Ouput and Its Variations, ed. O. R. White (Boulder: Univ. Colorado), 213
Walker, A. B. C., Jr. 1975, in Solar Gamma, X, and EUV Radiation, ed. S. R. Kane (Dordrecht: Reidel)
Walker, A. B. C., Jr., Barbee, T. W., Jr., Hoover, R. B., & Lindblom, J. F. 1988, Science, 241, 1781
Walker, A. B. C., Jr., DeForest, C. E., Hoover, R. B., & Barbee, T. W. 1993a, Sol. Phys., 148, 239
Walker, A. B. C., Jr., Hoover, R. B., & Barbee, T. W. 1993b, in Physics of Solar and Stellar Coronae, ed. J. Linsky (Dordrecht: Kluwer), 83
Walker, A. B. C., Jr., Lindblom, J. F., O'Neal, R. H., Allen, M. J., Barbee, T. W., Jr., & Hoover, R. B. 1990a, Opt. Eng., 29, 581
Walker, A. B. C., Jr., Lindblom, J. F., O'Neal, R. H., Hoover, R. B., & Barbee, T. W., Jr. 1990b, Phys. Scr., 41, 1053
Wang, Y.-M., & Sheeley, N. R. 1995, ApJ, 452, 457
Wang, Y.-M., et al. 1997, ApJ, 484, L75
Wheatland, M. S., Sturrock, P. A., & Acton, L. W. 1997, ApJ, 482, 510
Wilhelm, K., Lemaire, P., Dammasch, I. E., Hollandt, J., Schuehle, U., Curdt, W., Kucera, T., Hassler, D. M., & Huber, M. C. E. 1998, A&A, 334, 685
Woods, D. T. 1986, Ph.D. thesis, National Center for Atmospheric Research
Zweibel, E. G., & Boozer, A. H. 1985, ApJ, 295, 642